Al-Khwarizmi Engineering Journal, Vol. 14, No.2, June, (2018)
P.P. 40- 57

Al-Khwarizmi Engineering Journal

Transient Behavior Analysis for Solar Energy Storage in PCM-CFM Material Using Equivalent Heat Capacity Method as Storage Model

Talib K. Murtadha* **Hussien M. Salih**** **Ali D. Salman*****

** Department of Mechanical Engineering / College of Engineering /Mutah University/ Jordan*
*** Department of Electro-Mechanical Engineering / University of Technology / Iraq*
**** Department of Mechanical Engineering / University of Technology/ Iraq*
* Email: talib_km@yahoo.com
** Email: hussein_maj@yahoo.com
*** Email: aligaphory@yahoo.com

(Received 3 July 2017; accepted 7 November 2017)
https://doi.org/10.22153/kej.2018.11.003

Abstract

A paraffin wax and copper foam matrix were used as a thermal energy storage material in the double passes air solar chimney (SC) collector to get ventilation effect through daytime and after sunset. Air SC collector was installed in the south wall of an insulated test room and tested with different working angles (30º, 45º and 60º). Different SC types were used; single pass, double passes flat plate collector and double pass thermal energy storage box collector (TESB). A computational model based on the finite volume method for transient tw dimensional domains was carried out to describe the heat transfer and storage in the thermal energy storage material of collector. Also, equivalent specific heat method was employed to describe the heat storage and release in the mushy zone. Experimental results referred to an increase in thermal conductivity of paraffin wax that supported by copper foam matrix more than ten times. While the ventilation effect was still active for hours after the sun set, depending on the heat storage amount. Maximum ventilation mass flow rate with TESB collector was recorded with value equals to 36.651 kg/hr., when the overall discharge coefficient that was calculated for the system equals to 0.371. Experimental results showed that the best working angle range was 45~60º, and the highest air to the collector approaching temperature appeared to the double passes flat plate collector. Results gave greater heat storage efficiency of (47)% when the maximum solar radiation was 780 W/m^2 at 12.00pm, while the energy summation through duration charge time was 18460 kJ. Computational results, depending on the equivalent heat capacity method for heat storage or release from phase change material that supported by copper foam matrix, showed the behavior of paraffin wax melting and solidification situation through periodic for charge and released heat from the solar collector. Also, these results gave agreement approaching the experimental results for the heat storage in the combined heat storage material, with standard error of 16.8%.

Keywords: *CFD, Copper foam matrix, Heat storage, Paraffin wax, Phase change material, Solar chimney.*

1. Introduction

There are many studies carried out to decrease the percentage of the carbon release by consumption from traditional energy, and that is done by employing the renewable energy. Solar irradiance is one of the most important energy sources, especially in the day time. But, the decrease in the solar irradiance near the sunset, or absence of the energy after sunset, lead to searching for a method to store the thermal energy through day time and release it after sunset or in the night time. H. Kotani et al. [1] developed a SC with built-in latent heat storage material for Sodium Sulfate Decahydrateto induces natural ventilation in evening and night. The simulated and experimental results showed that the integration of (PCM) as heat storage inside the SC was effective. It can supply nearly constant air flow rate of 155 m^3/h, in evening and night, in condition when the PCM is completely melting during the day. M. B. Al-Hadithi [2] conducted a numerical simulation for a case study of air conditioning in two walls type, employing two types of walls; treated wall (TW) with phase change material (75% Iraqi cement+25%PCM), and non-treated wall (NTW). Numerical results of TW produced lower surface temperature and heat flux towards the cooling space to NTW. Alkilani, Mahmud et al. [3] represented a theoretical investigation for a compound of paraffin wax with 5%Aluminum powder, to use it as thermal energy storage in a solar air heater. The air was heated by pumping air through a row of cylinders, where the compound of TES materials stored. Results showed that for different TES phases, the increasing of airflow over TES's cylinders leads to decrease the outlet air temperature. In addition, the reduction in airflow rate leads to increase the freezing time of TES compound. M. E. Poulad, A. Fung [4] used a thermosyphon with phase change material panel (TP-system), to transfer the heat through thermpsyphon to the PCM as storage heat and use later. A model for one dimension, steady state was analyzed. Results of TP system showed that more than 10^6 W. hr./m^2 from energy was transferred to the test building annually in Toronto city, also results referred to that the insulated surface temperature of TP in the coldest month could be increased to 54.4 °C. K. E. Amori and S. Watheq [5] represented a numerical and experimental study for SC that was designed, manufactured and tested the effect of paraffin wax that employed in the SC's collector. A mathematical model of CFD was solved by using FVM to predict the thermal performance for SC under transient condition. Other different parameters were studied. Results showed that by adding the PCM to the SC lead to extend the ventilation period, so the effect of SC on the ventilation was appeared not only in the day time, but also in the night time. P. H. Vadwala[6] investigated a method for enhancing the thermal conductivity of the PCM like paraffin wax, by supporting the PCM by open metal foam. Results referred to increase the PCM thermal conductivity by 16-18 times.

2. Experimental Set-up

2.1. Rig Set-Up

Three different types of the solar chimney were tested with ventilation mode. SCs types are single pass and double pass flat plate collector, and double pass TESB collector. Those different SCs were installed to the south wall of the insulated test room. To enhance heat transfer inside thermal storage material for tilted SC, so semi refined paraffin wax with melting temperature (48~54°C) was supported by copper foam matrix with 95% porosity and ppi equal 30. A vertical preheat SC with fully refined paraffin wax and CFM were installed before the tilted SC with ($T_m =$ 58~62°C). The vertical SC was supported by the array of an evacuated tubular collector with a thermosyphon to collect the solar irradiance and charge TES material. Also a direct irradiance was collected by the face surface of vertical TESB collector, as shown in Fig. (1, 2, and 3).

2.2. Measurement and Instruments Tools

Data acquisition system with more than 100 thermocouple probes was used to read the temperature of the collector surface, inside thermal storage material, the temperature of the air through the SC, transparent acrylic cover and else. Also, a high accuracy digital anemometer was employed to measure the air velocity in different locations and different levels through solar chimney gap. Modern solar intensity readers with weather station were installed to the test room.

2.3. Effective Dimensions of the System

The most important effective dimension was the aspect ratio (ar) of SC (ratio of solar chimney length to its gap). The ar design value was depending on the optimum value at 12/1. So, the final design value for ar equals 25/1 for single pass SC and 50/1 for each pass of double passes SC. Depending on the designed value of ar, Fig.2, so other dimensions of SC will be limited. For tilted SC, the length was 1.5 m, width 0.75 m, chimney gap equals 6 cm in a single pass, and 3 cm for eachpass in the double passes SC. The thermal energy storage box (TESB) (PCM-CFM) in vertical SC has dimensions 1*0.75*0.025 m, while the tilted TESB has dimensions 1.5*0.75*0.025 m, and the weight factor (wax/combined) represents 59.48%.The insulated test room has dimensions (2*1.5*1.5) m in length, width and height, supported by SCs in the south wall. Length of test room is bigger than width and height, to clarify the behavior of temperature distribution inside test room. The structure of test room consists of a wooden frame, insulated by cork and glass wool.

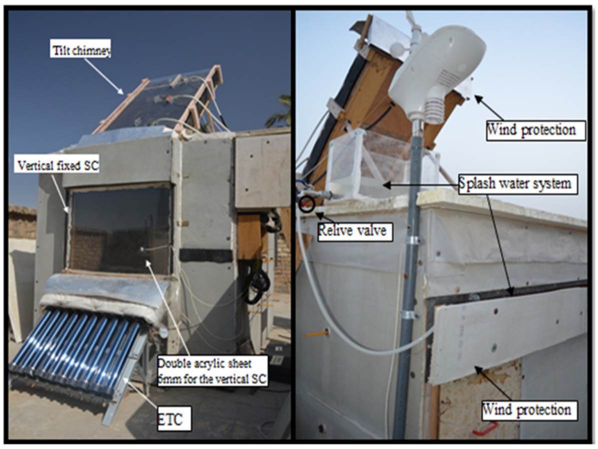

Fig. 1. Test room with a vertical and tilted SC that used (PCM-CFM) as thermal energy storage material.

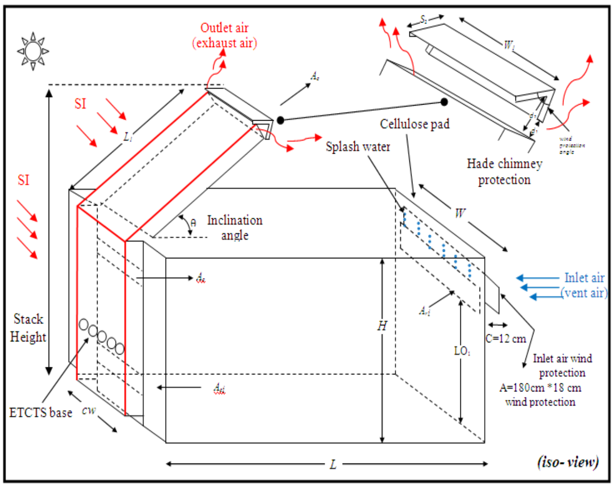

Fig. 2. Schematic diagram of insulated test room with ventilation, ventilation and evaporative cooling modes.

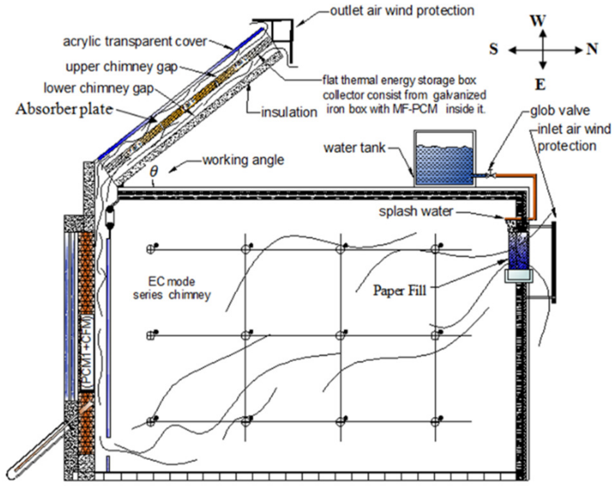

Fig. 3. Schematic diagram describing the test room in ventilation and evaporative cooling mode depicting the vertical and tilted solar chimney with thermal energy storage box.

2.4. The Solar Chimney (SC)

The system of ventilation that used SC consisted of vertical SC and tilted SC, both of them are connected in series. Vertical solar chimney (preheat SC) depended on the evacuated tubular collector with a thermosyphon beside the transparence covered collector was employed to collect heat from solar irradiance, Fig.3.In vertical collector; heat storage is inside the combined of PCM-CFM. In the tilted SC, three different types of collector were used as mentioned previously. Single pass flat plate collector is showing in Fig.5, double passes flat plate collector in Fig.6, and double passes flat thermal energy storage box collector in Fig.7. The third collector depended on the PCM-CFM to store heat and release it after sun-set.

3. Computational Model for Transient Heat Storage

The physical model and numerical solution for transient conduction of heat storage represent the absorbed heat from the solar radiation and then store it in the thermal energy storage box (PCM-CFM). Transient heat transfer inside TESB by conduction is predominating, to heat transfer by convection from the outer surface of the storage box, especially the air side of chimney gap. All properties of air, acrylic and effective properties for paraffin wax and CFM are mentioned as shown below, where An Effective Heat Capacity Method was employed to estimate the PCM and CFM heat storage in phase change material.

Physical models and the governing equation (in a transient state) were employed by the FVM with explicit scheme over a control volume (CV), Fig.10, to construct the main program of the numerical model for heat transfer simulation in thermal energy storage box. Below is mathematical modeling and steps of solution for transient part of simulation program.

3.1.Thermal Energy Storage Material

Heat energy was stored and released it inactive time, thereby must be transferred in limited duration time, and that means to limit the value of thermal conductivity of the storage material. So, a CFM with 95% porosity and 30 ppi was used to support the main storage material (paraffin wax), Fig.4.

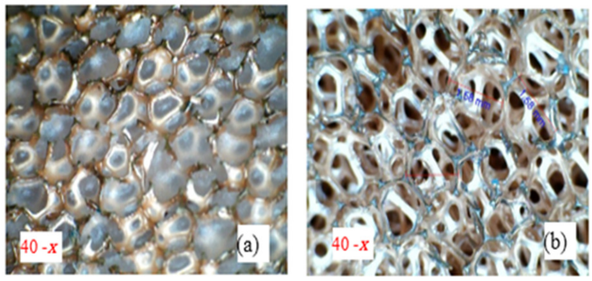

Fig. 4. Copper foam matrix a-with PW, b-without PW.

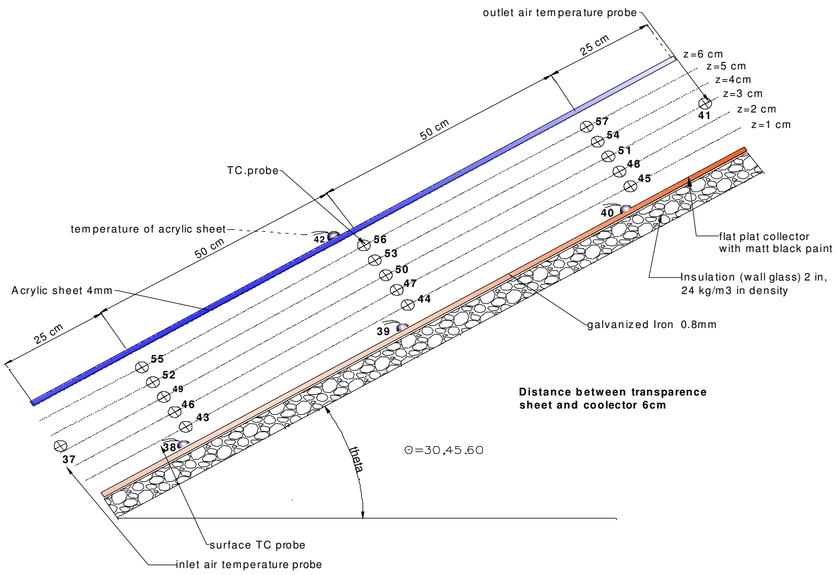

Fig. 5. Single pass tilted solar chimney with flat plate collector.

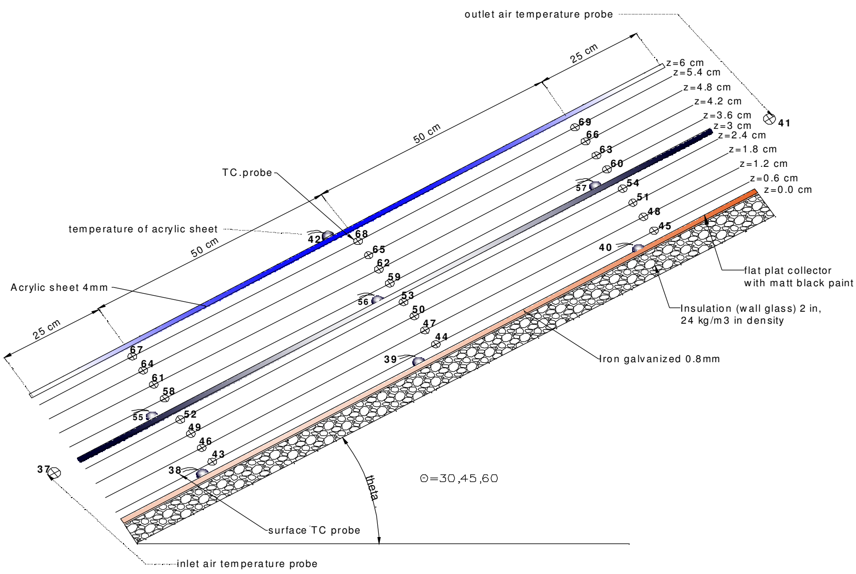

Fig. 6. Double passes tilted solar chimney with flat plate collector.

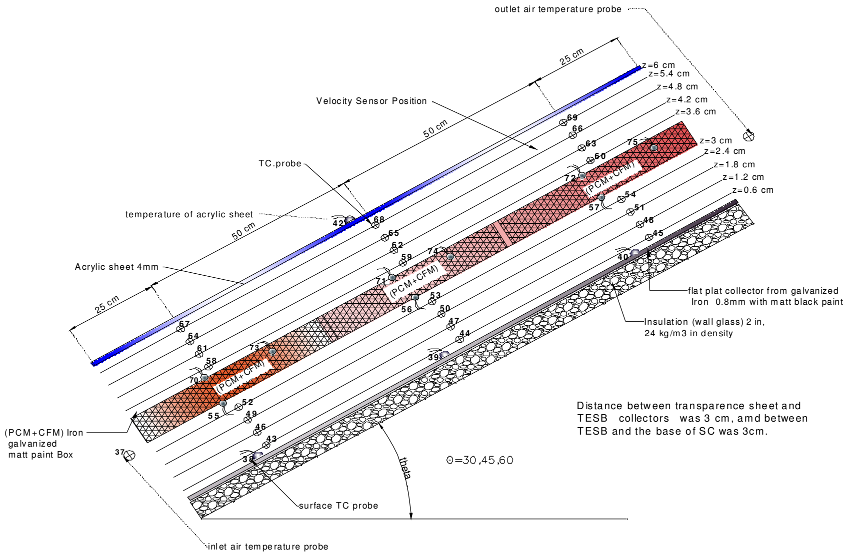

Fig.7. Double passes tilted solar chimney with thermal energy storage collector.

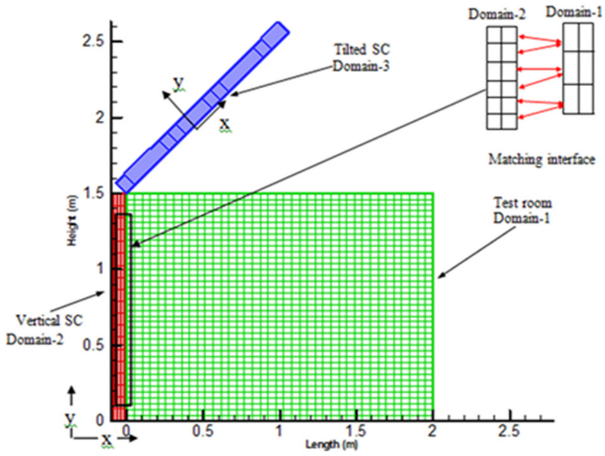

Fig. 8. Mesh grid domains matching.

3.1.1 Effective Thermal Conductivity

To define the effective thermal conductivity for the combined PCM-CFM as shown in the equations below [7, 8and 9]. Averaging the thermal conductivity of each section on the basis of the conductivities is down in the following manner:

$$k_n = \frac{V_{n,s}k_s + (V_n - V_{n,s})K_f}{V_n} \qquad \ldots(1)$$

this thermal conductivity is calculated for each section (n: A, B, C, D). The thermal conductivity through the representative section is calculated based on heat conduction through a series of four levels using Fourier's law of heat conduction to give the relation.

$$k_{eff} = \frac{L_A + L_B + L_C + L_D}{\left(\frac{L_A}{k_A}\right) + \left(\frac{L_B}{k_B}\right) + \left(\frac{L_C}{k_C}\right) + \left(\frac{L_D}{k_D}\right)} \qquad \ldots(2)$$

By substituting the equation for the section lengths (L_n), the thermal conductivities for each (k_n), and the positive solution for d from eqn. (3)

$$d = \sqrt{\frac{\sqrt{2}\left(2 - \left(\frac{5}{8}\right)e^3\sqrt{2} - 2\varepsilon\right)}{\pi\left(3 - 4e\sqrt{2} - e\right)}} \qquad \ldots(3)$$

yields a lengthy equation for the effective thermal conductivity as a function of the porosity, e, and d (which is a solved function of ε and e from eqn.(4)

$$\varepsilon = 1 - \frac{\sqrt{2}}{2}\left(de^2 + \frac{1}{2}\pi d^2(1-e) + \left(\frac{1}{2}e - d\right)e^2 + \pi d^2\left(1 - 2e\sqrt{2}\right) + \frac{1}{4}e^3\right) \qquad \ldots(4)$$

Introducing the simplifying notation gives,

$$R_A = \frac{4d}{(2e^2 + \pi d(1-e))k_s + (4 - 2e^2 - \pi d(1-e))k_f} \qquad \ldots(5)$$

$$R_B = \frac{(e-2d)^2}{(e-2d)e^2 k_s + (2e - 4d - (e - 2d - (e-2d)e^2)k_f} \qquad \ldots(6)$$

$$R_C = \frac{(\sqrt{2} - 2e)^2}{2\pi d^2\left(1 - 2e\sqrt{2}\right)k_s + 2\left(\sqrt{2} - 2e - \pi d^2\left(1 - 2e\sqrt{2}\right)\right)k_f} \qquad \ldots(7)$$

$$R_D = \frac{2e}{e^2 k_s + (4 - e^2)k_f} \qquad \ldots(8)$$

Finally, this yields the final result of the effective thermal conductivity to be:

$$\bar{k}_{PCM-MF} = \frac{\sqrt{2}}{2(R_A + R_B + R_C + R_D)} \qquad \ldots(9)$$

where $e = 0.339$, k_s: Thermal conductivity of the material used to manufacture the metal foam.k_f: Thermal conductivity of the material saturated inthe metal foam. R_A, R_B, R_C and R_D: Thermal resistance of four different layers inside a tetrakaidecahedron cell.

The effective thermal conductivity $\bar{k}_{PCM-MF}$is a result of these four thermal layers placed in parallel.

Other properties of the combined, like density and specific heat that can be estimated from the general equations as shown below [6]:

$$\varphi_{eff} = (1-\varepsilon)\varphi_x + \varepsilon\,\varphi_y \qquad \text{... (10)}$$

$$\varphi_{eff-x} = (1-\varepsilon)\varphi_{Px} \qquad \text{... (11)}$$

$$\varphi_{eff-y} = \varepsilon\varphi_{Px} \qquad \text{... (12)}$$

$\varphi =$ Physical properites, $\varepsilon =$ CFM porosity or porosity of material, $x, y =$ Material type

3.1.2 Equivalent Heat Capacity

To calculate the effective specific heat for pure paraffin wax in the mushy zone (tow phase area), Fig.9, as shown below;

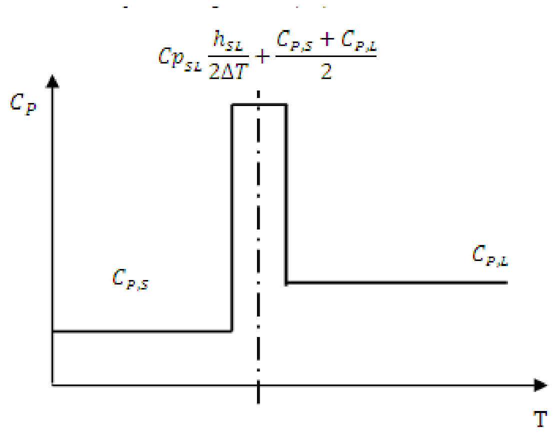

Fig. 9. Specific heat value for paraffin wax in solid liquid and mushy zone.

$$C_{P-eff} = \frac{h_{s-l,wax}}{\Delta T_{mushy}} + C_{P,av} \qquad \text{... (13)}$$

$$C_{P,av} = \tfrac{1}{2}\left(C_{P,S} + C_{P,l}\right) \qquad \text{... (14)}$$

So, by defining the Equivalent Heat Capacity Method,

$$C_P = \begin{cases} C_{P,S} & T < T_m - \Delta T \\ C_{P,SL} & T_m - \Delta T < T < T_m + \Delta T \\ C_{P,L} & T > T_m + \Delta T \end{cases} \qquad \text{... (15)}$$

If the latent heat of fusion is known, and specific heat for solid and liquid with ΔT, so the specific heat of mushy zone equation (13)can be defined as shown in Fig.9.

3.2 Governing Equation Applied

To describe the governing equation in conduction heat transfer for combined material as shown below in Fig.10, [10, 11and 12];

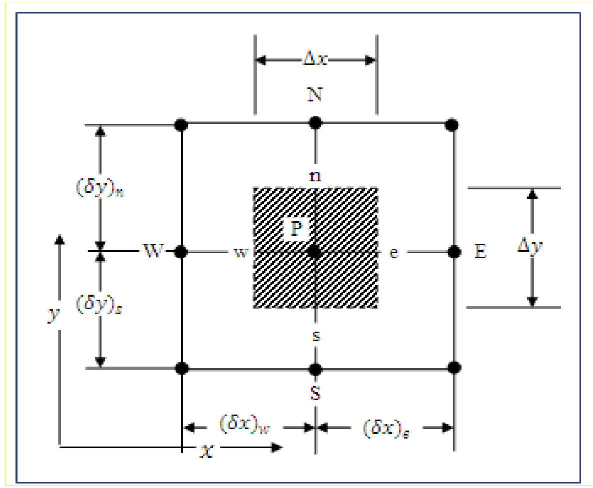

Fig. 10. Control volume for the two- dimensional control volume.

$$\rho c_p \frac{\partial T}{\partial t} = \left(k\frac{\partial^2 T}{\partial x^2} + k\frac{\partial^2 T}{\partial y^2}\right) + q'' \qquad \text{... (16)}$$

$\alpha = \frac{k}{\rho\, c_p}$, α is the diffusivity for storage material, like wax, foam matrix, galvanized steel, and acrylic. For the discretized the cell, and by the transient part of two dimensional for left hand side equation, and the heat generation in right hand side equation. The integration of both sides gives:

$$\begin{aligned} T_p = T_p^{old} + rr^n\Big\{ & k\frac{\Delta y}{\Delta x}\Big|_e T_E - k\frac{\Delta y}{\Delta x}\Big|_e T_P \\ & + k\frac{\Delta y}{\Delta x}\Big|_w T_W - k\frac{\Delta y}{\Delta x}\Big|_w T_P \\ & + k\frac{\Delta x}{\Delta y}\Big|_N T_N - k\frac{\Delta x}{\Delta y}\Big|_N T_P \\ & + k\frac{\Delta x}{\Delta y}\Big|_S T_S - k\frac{\Delta x}{\Delta y}\Big|_S T_P \\ & + \Delta y q\Big\} \end{aligned} \qquad \text{... (17)}$$

$rr^n = \frac{\Delta t}{\Delta x\, \Delta y\, \rho c_P}$,

Assume

$a_E = k\frac{\Delta y}{\Delta x}\Big|_e$, $a_W = k\frac{\Delta y}{\Delta x}\Big|_w$, $a_N = k\frac{\Delta x}{\Delta y}\Big|_n$, $a_S = k\frac{\Delta x}{\Delta y}\Big|_s$

a_E, a_W, a_N, a_S:are the coefficients in the discretization equation.

Let $a_P = (\,a_E + a_W + a_N + a_S)$, $a_P$is the coefficient in the discretization equation at the mean point.

$$\therefore\ T_p = T_p^{old} + rr^n\{a_E T_E + a_W T_W + a_N T_N + a_S T_S - a_P T_P + \Delta y\, q\} \qquad \text{... (18)}$$

With converge criteria for explicit scheme,

$$\left(\frac{\alpha\,\Delta t}{\Delta x^2} + \frac{\alpha\,\Delta t}{\Delta y^2}\right) < \frac{1}{2} \qquad \text{...(19)}$$

The combined conduction- convection heat transfer over the control volume is shown in Fig.11, as a sample [13 and 14], so the summation of heat at each node equals zero.

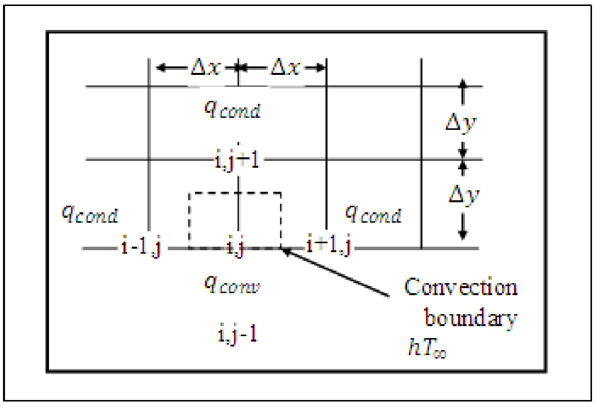

Fig. 11. Grid points for rectangular grid system with conduction- convection heat transfer over CV.

$$\sum all\ side\ \ q = q_E + q_W + q_N + q_S + S \quad ...(20)$$

$$\frac{\Delta x\ \Delta y\ \rho C_P}{\Delta t}\left(T^n_{(i,j)} - T^o_{(i,j)}\right) = q_E + q_W + q_N + q_S + S \quad ...(21)$$

Let face area of CV in x-direction $a_x = \Delta y$, Let face area of CV in y-direction $a_x = \Delta y$

$$\left.\begin{aligned} q_E &= k_e\, A_e \frac{\left(T_{i+1,j} - T_{i,j}\right)}{\Delta x}, \\ q_W &= k_w\, A_w \frac{\left(T_{i-1,j} - T_{i,j}\right)}{\Delta x} \\ q_N &= k_n\, A_n \frac{\left(T_{i,j+1} - T_{i,j}\right)}{\Delta y}, \\ q_S &= h_{conv} A_s \left(T_{i,j-1} - T_{i,j}\right) \end{aligned}\right\} \quad ...(22)$$

$A_e = A_w = a_x$, so $A_n = A_s = a_y$

Applying the general equation gives,

$$\frac{\Delta x\ \Delta y\ \rho C_P}{\Delta t}\left(T_p - T_p^{old}\right) = q_E + q_W + q_N + q_S + S \quad ...(23)$$

By discretizing the conduction equation, all partial values convert to the difference value. Then the final equation for conduction convection heat transfer becomes;

$$T^n_{(i,j)} = T^o_{(i,j)} + rr^n\{a_E\left(T_{i+1,j}\right) + a_W\left(T_{i-1,j}\right) + a_N\left(T_{i,j+1}\right) + a_S\left(T_{i,j-1}\right) - a_P\left(T_{i,j}\right)_P + \Delta yq\} \quad ...(24)$$

Equation above represents the general form of heat transfer over the CV and it needs to apply the initial and BC. If no heat generation and no heat exposure to the CV side, then the source term of heat is equal to zero. Building and running the simulation program need to employ the general form of energy equation-24, by defining the initial and BC over the CV shape for the vertical TESB in Fig.12,and tilted one, as shown in Fig.13, and then tabulating the nodes relationships between each other's. Then, the iteration solvers are used after defining the main equation coefficients, to solve this equation over the limit of finite CV for the selective nodes. To define the coefficients of equation-24, for heat transfer by conduction or for heat storage in materials, so it must to define the properties of materials consist of the galvanized steel, acrylic, copper foam matrix and the properties of paraffin wax at solid and liquid state. To simplify the computational model, the physical fact that the phase change taken place in a temperature interval ($T_m \pm \Delta T_m$) can be employed. So, the heat balance equations that describe the heat storage and heat transfer during phase change can be divided as regions state: solid, liquid and mushy zone.

For solid phase or state,$\rho_s, C_{P,s}, k_s$

$$T < T_m - \frac{\Delta T_m}{2} \quad ...(25)$$

For liquid phase,$\rho_l, C_{P,l}, k_l$

$$T > T_m - \frac{\Delta T_m}{2} \quad ...(26)$$

For mushy zone,$\rho_m, C_{P,m}, k_m$

$$T_m - \frac{\Delta T_m}{2} \le T \le T_m + \frac{\Delta T_m}{2} \quad ...(27)$$

Many methods are defined to describe the phase change. The effective heat capacity method is the one of the simplest and effective method to estimate the heat transfer or heat storage in the different three regions. With narrow temperature difference in mushy zone, this method depicts the most precise method.

3.3 Effective Heat Capacity Method

In this method, the latent heat effect is expressed as a finite temperature dependent on the specific heat that occurs over the temperature range.In this method, it is possible to describe the non-isothermal phase change. So, the effective (equivalent) heat capacity during the phase change can be presented as shown in the equation [15]:

$$C_{P,eff} = \frac{h_{sl}}{\Delta T_m} + C_{P,av} \quad ...(28)$$

ΔT_m is the mushy zone diffrence temperature, and h_{sl} means the value of latent heat of fusiont o define the average heat capacity $C_{P,av}$,

$$C_{P,av} = \frac{1}{2}\left(C_{P,s} + C_{P,l}\right) \quad ...(29)$$

For incompressible fluid and for solid, it is possible to change C_P instead of C_V as shown above and with acceptable error.

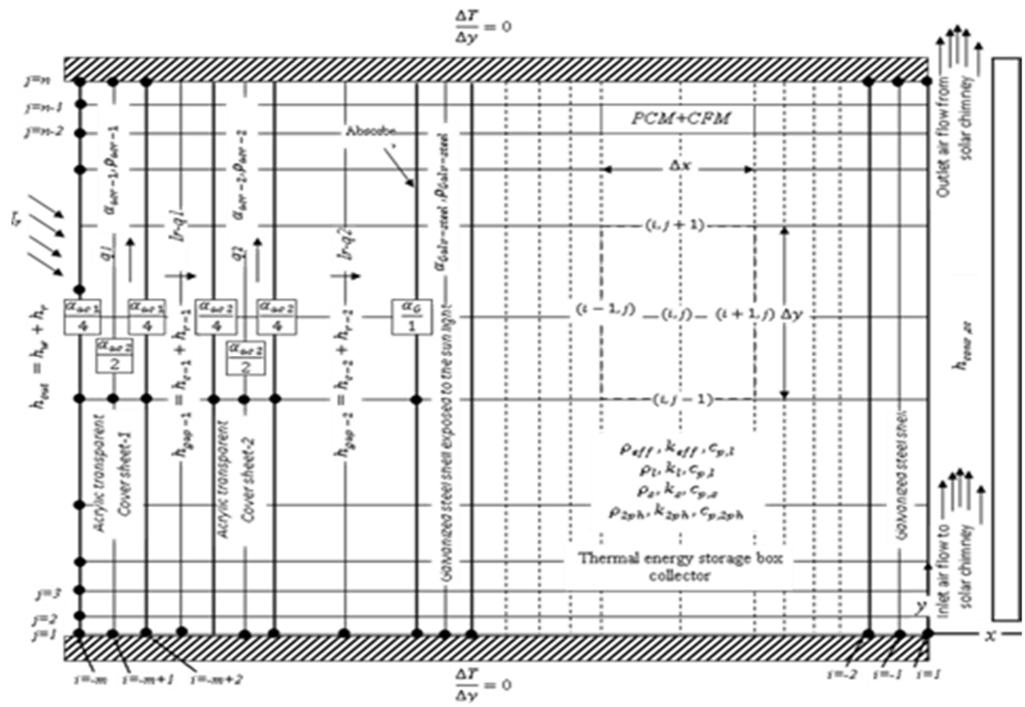

Fig. 12. Scheme of vertical solar chimney with grid point and boundary conditions and PCM-CFM storage material.

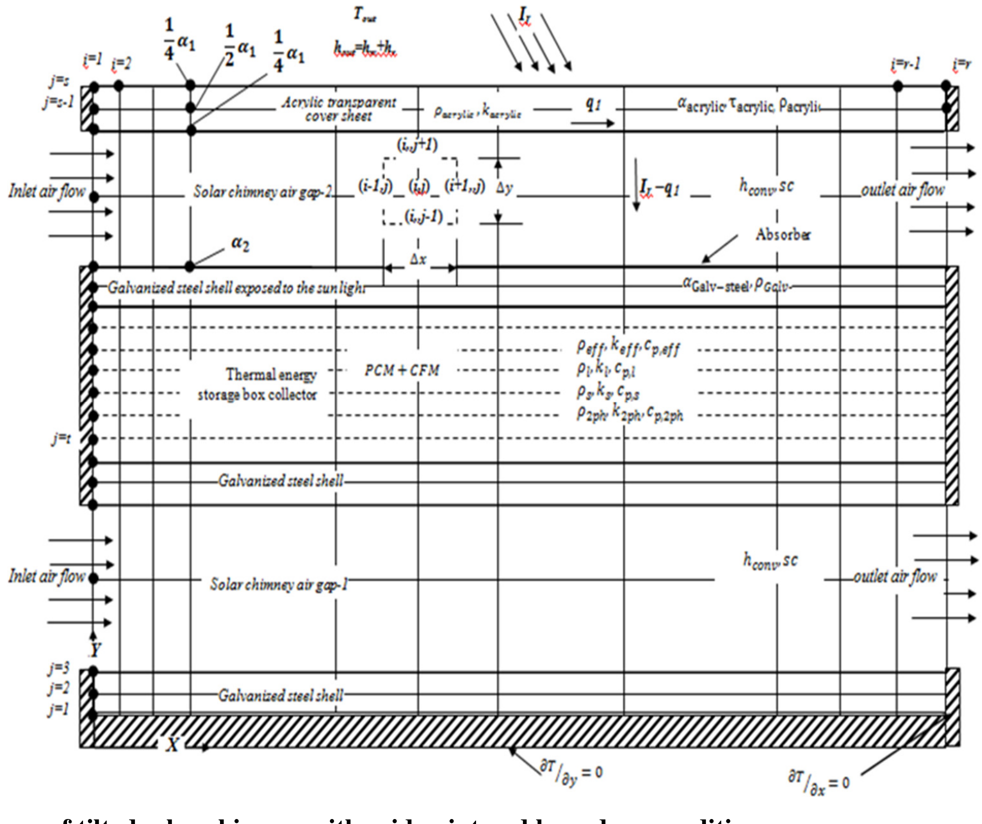

Fig. 13. Scheme of tilted solar chimney with grid point and boundary conditions.

To define the new set of properties of PCM by melting process for a small unit volume, Fig.14 shows the time-dependent temperature of unit volume of phase change material during T_1 to T_2. The density of PCM can be estimated by arithmetic average:

$$\rho_m = \frac{1}{2}(\rho_s + \rho_l) \quad at\ T_m - \frac{\Delta T_m}{2} \leq T$$

$$\leq T_m + \frac{\Delta T_m}{2} \quad \dots(30)$$

For the compound of copper foam matrix and phase change material, the density can be defined as:

$$\rho_{PCM-CFM} = (1-\varepsilon)\rho_{CFM} + \varepsilon\rho_{PCM} \quad \dots(31)$$

For pure PCM, it is defined as:

$$k_m = \frac{1}{2}(k_s + k_l) \quad at\ T_m - \frac{\Delta T_m}{2} \leq T \leq T_m + \frac{\Delta T_m}{2} \quad \dots(32)$$

While, the thermal conductivity is defined in mushy zone as shown in below for the compound of the PCM-CFM, as effective value. The specific heat can be defined for the PCM-CFM as:

$$C_{P,PCM_m-CFM} = (1-\varepsilon)C_{P,CFM} + \varepsilon C_{P,PCM_m} \text{at} T_m - \frac{\Delta T_m}{2} \leq T \leq T_m + \frac{\Delta T_m}{2} \quad \dots(33)$$

$$\varepsilon = \frac{\text{bulk volume} - \text{metal volume}}{\text{bulk volume}} 100\% = \text{porosity}$$

3.4 Energy Storage and Release

By defining the new properties of the heat storage material, the storage or release energy in a control volume of the compound q^V may be expressed as:

$$q^V = \int_{T_i}^{T_1} \rho_s\, C_{P,s}\, dT + \int_{T_1}^{T_2} \rho_m\, C_{P,m}\, dT + \int_{T_2}^{T_l} \rho_l\, C_{P,l}\, dT \quad \dots(34)$$

$$q^V = \varepsilon \int_{T_i}^{T_1} \rho_{s-PCM}\, C_{P,s-PCM}.dT + (1-\varepsilon)\int_{T_i}^{T_1} \rho_{CFM}\, C_{P-CFM}.dT + \varepsilon \int_{T_1}^{T_2} \rho_m\, C_{P-m}.dT + (1-\varepsilon)\int_{T_1}^{T_2} \rho_{CFM}\, C_{P-CFM}.dT + \varepsilon \int_{T_2}^{T_l} \rho_{l-PCM}\, C_{P-PCM}.dT + (1-\varepsilon)\int_{T_2}^{T_l} \rho_{CFM}\, C_{P-CFM}.dT \quad \dots(35)$$

$$q^V = \{\varepsilon(\rho_{s-PCM}C_{P,s-PCM}) + (1-\varepsilon)(\rho_{CFM}C_{P-CFM})\}(T_1 - T_i) + \{\varepsilon(\rho_m C_{P-m}) + (1-\varepsilon)(\rho_{CFM}C_{P-CFM})\}(T_2 - T_1) + \{\varepsilon(\rho_{l-PCM}C_{P,l-PCM}) + (1-\varepsilon)(\rho_{CFM}C_{P-CFM})\}(T_l - T_2) \quad \dots(36)$$

$$T_1 = T_m - \frac{\Delta T_m}{2}, \quad T_2 = T_m + \frac{\Delta T_m}{2},$$

$$T_1 - T_i = T_m - \frac{\Delta T_m}{2} - T_i \quad \dots(37)$$

$$T_2 - T_1 = T_m + \frac{\Delta T_m}{2} - T_m + \frac{\Delta T_m}{2} = \Delta T_m \quad \dots(53)$$

$$T_l - T_2 = T_l - T_m - \frac{\Delta T_m}{2} \quad \dots(38)$$

$$q^V = \{\varepsilon(\rho_{s-PCM}C_{P,s-PCM}) + (1-\varepsilon)\left(\rho_{CFM}C_{P-CFM})\right\}\left(T_m - \frac{\Delta T_m}{2} - T_i\right) + \left\{\varepsilon\left(\frac{\rho_m h_{ls}}{\Delta T_m}\right) + \frac{\rho_{s-PCM}C_{Ps-PCM} + \rho_{l-PCM}C_{Pl-PCM}}{2} + (1-\varepsilon)(\rho_{CFM}C_{P-CFM})\right\}(\Delta T_m) + \{\varepsilon(\rho_{l-PCM}C_{P,l-PCM}) + (1-\varepsilon)(\rho_{CFM}C_{P-CFM})\}\left(T_l - T_{m-}\frac{\Delta T_m}{2}\right) \quad \dots(39)$$

By assuming no big change in the properties at the same material constant values, $\rho_{CFM}, C_{P-CFM}, \rho_{l-PCM}, \rho_{S-PCM}, C_{P,s-PCM}, C_{P,l-PCM}, \varepsilon, T_m, \Delta T_m$, can be entered in the subroutine- program as general constants.

Let

$$\left.\begin{array}{l} x_1 = \varepsilon(\rho_{s-PCM}C_{P,s-PCM}), \\ x_2 = (1-\varepsilon)(\rho_{CFM}C_{P-CFM}), \quad x_3 = \varepsilon\rho_m h_{ls} \\ x_4 = \dfrac{\rho_{s-PCM}C_{Ps-PCM} + \rho_{l-PCM}C_{Pl-PCM}}{2}, \\ x_5 = \varepsilon(\rho_{l-PCM}C_{P,l-PCM}) \end{array}\right\} \quad \dots(40)$$

Equation (39) can be re-written as:

$$q^V = \left\{(x_1 + x_2)\left(T_m - \frac{\Delta T_m}{2} - T_i\right)\right\} + \left\{\left(\frac{x_3}{\Delta T_m} + x_4 + x_2\right)\Delta T_m\right\} + \left\{(x_5 + x_2)\left(T_l - T_m - \frac{\Delta T_m}{2}\right)\right\} \quad \dots(41)$$

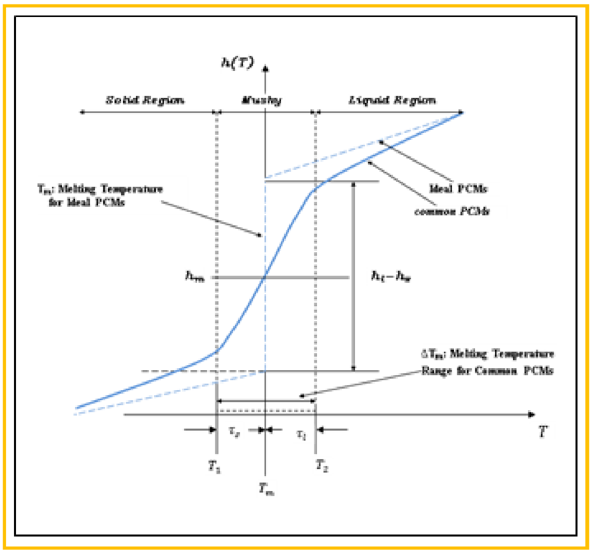

Fig. 14. Mushy zone for phase change material.

3.5. Simultaneous Efficiency of Heat Storage

To compute the simultaneous efficiency at the duration time of heat charge, by compute the rate of heat storage in TESB during its exposure to the solar radiation which can be calculated from the eqn. below [15];

$$q = \frac{m\Delta h}{t} = m_{wax}\Delta h_{wax} + m_{copper}C_{copper}\Delta T_{copper} \quad \dots(42)$$

Where, m= mass for wax and copper foam matrix.
t= duration time to charge TESB by heat (q).
So, the heat storage in the duration time t can be found from eqn. (43

$$Q = q.t \quad ..(43)$$

The heat storage during the duration charge for N time, can be computed by algebraic summation of eqn. 14 to get

$$Q_{total} = \sum_{n=1}^{N}\{m_{wax}\Delta h_{wax} + m_{copper}C_{copper}\Delta T_{copper}\} \quad \dots (44)$$

Thus, the ratio of the heat storage to the heat absorbed by TESB is

$$\eta = \frac{Q_{storage}}{Q_{absorbed}} = \frac{\{m_{wax}\Delta h_{wax} + m_{copper}C_{copper}\Delta T_{copper}\}}{I_{beam}.A_a.\alpha_a.t} \quad \dots (45)$$

4. The Computational Solution

The physical model and numerical solution for transient conduction of heat storage present the heat collecting from the sun radiation (in the tilted solar chimney).The heat is collected and store in the thermal energy storage box (paraffin wax with copper foam matrix). Heat transfer in un-steady state inside TESB by conduction is predominating, with respect to heat transfer by convection from the outer surface of the storage box (air side), especially the side of chimney gap, matching between conduction and convection domain was depicted in the mush grid, Fig.8. All properties of air, acrylic and effective properties for paraffin wax and copper form matrix are defined in the coefficients of general equation-39, where an Equivalent Heat Capacity Method is employed. The main computer program written by FORTRAN-95 language consists of two parts, room domain and SCs parts, while matching among three mesh grid domains is employed to transfer computational data between each other's, Fig.8.

5. Experimental Test Procedure

The experimental work was achieved in June, 2015, where data are logging for the dependent variables along 12 hours. All measurements and instruments tools were used as mentioned previously to measure and record the dependent variable, for each 2 hours as test interval, and average value for general variables that measured and recorded by WS data logger along 24 hours, with 20 minutes as test interval. Measuring temperature was in chimneys gap, test room space, TESB and outdoor temperature.

6. Theoretical Consideration

In this study, assuming there are no heat losses directly from test room to the surround, or from the insulated parts of SC's. So, according to the heat balance, heat absorbed by collector must be equal to heat released to the working air that passes through the chimney gap.

7. Results and Discussion

Experimental results show the practicability to employ the porous material like the CFM to increase the heat transfer in the PCM. Fig.15. depicts the profile temperature of heat rejection from two samples for paraffin wax with and without CFM, the sample of PCM without CFM rejects heat in short time comparing with the other sample. Figs.16, 17 and18 show the SC absorber temperature for the three different SC collectors, the highest temperature appears in the absorber for single SC collector, and that does not mean, essentially, efficient SC collector as shown later in the efficiency of approaching results, on the other side, the results refer to the high efficient for double passes flat plate collector with high approaching between air to absorber temperature with the best working angle at range (45°~60°), while the double passes TESB collector refers to

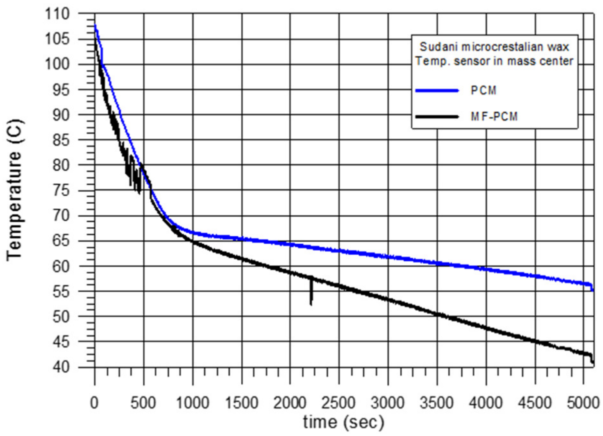

Fig. 15. Solidification behavior of microcrestalian wax with the temperature sensor in the center of wax body, with and without foam matrix.

The good approaching between air to absorber temperature with the longest duration time from other two collectors. Fig.19, presents the absorber temperature for different SCs at 30° in tilted angle. It's clear that the best efficiency is with the double passes SC collector, where low temperature appears according to the air temperature in Figs.(25, 26 and 27), and that means higher approaching between air to the absorber of SC. Other comparisons in angles 45° and 60°, Fig.20 and Fig.21 for three types of SC are represented, referring to the same conclusion with respect to the 60° as the best tilted working angle. Fig, (22, 23 and24) reveal the comparison results between the absorber and wax temperature in different sections of the TESB collector and refer of the efficient angle at 60°.Fig.28, shows the solar radiation, energy summation and heat storage efficiency, and the results lead to the highest heat storage efficiency 46.5% occurred at the higher solar radiation 783 W/ m^2.Fig.29, refers to the error in results when the efficiency of approaching in temperature between air to absorber in the TESB collector was bigger than 100%, but the logical explanation refers to the increase in air temperature that comes from the vertical SC, while the absorber of TESB was still storage heat energy, so it is still with low temperature from than the air and that is opposite to what happened with the single pass SC.

Other un-logical behavior of the efficiency approaching for single pass SC is bigger than 100% after sun-set and that logically happened because the back flow in the chimney hood caused decreases in the absorber temperature, other results for TESB SC are depicted in Fig.30. The computational results are shown in Fig.31 that depicts the temperature distribution in the heat storage material (PCM-CFM) through test day. The wax variation temperature in TESB, compared with Fig.22, gives a good approaching between the results with highest relative error 16.8%. Also, the computational results appeared the highest temperature of TESM in the middle of the outside face of thermal energy storage solar collector.

8. Conclusion

Heat storage in the phase change material like wax is not efficient, because there is a bad (low) thermal conductivity for the wax and that means bad heat transfer when heat storage and release in sensible or latent phase or in both phases. To enhance the thermal conductivity, it is effective to employ CFM with high porosity to enhance heat transfer through the compound as shown in the results. Heat storage in the combined material still releases heat energy after absence the heat source, and that refers to success for employing the paraffin wax with copper foam matrix as a thermal energy storage material. Computational model, depending on equivalent specific heat method and numerical solution, gave an agreement result for the heat storage in the combined material. Computational results appeared a logical and agreement behavior for melting and solidification in the combined heat storage material.

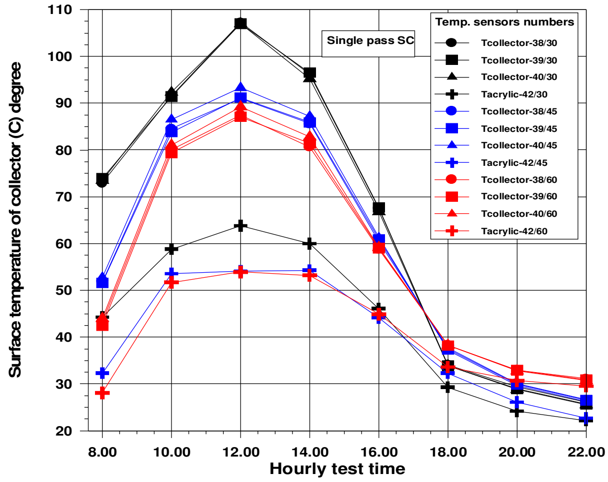

Fig. 16. Comparison between the SC absorber temperature for single pass, and with different tilted angles.

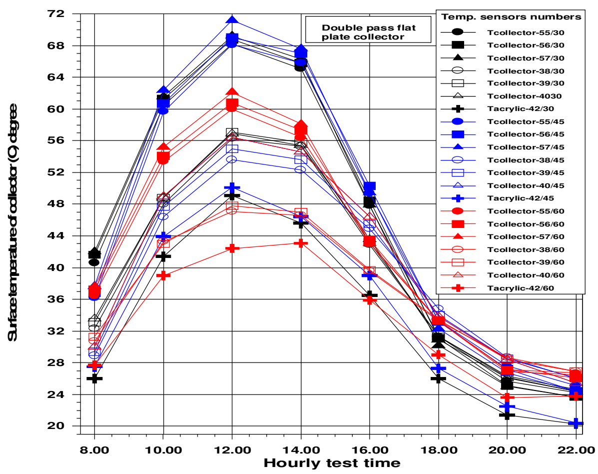

Fig. 17. Comparison between the SC absorber temperature for double passes flat plate collector and with different tilted angles.

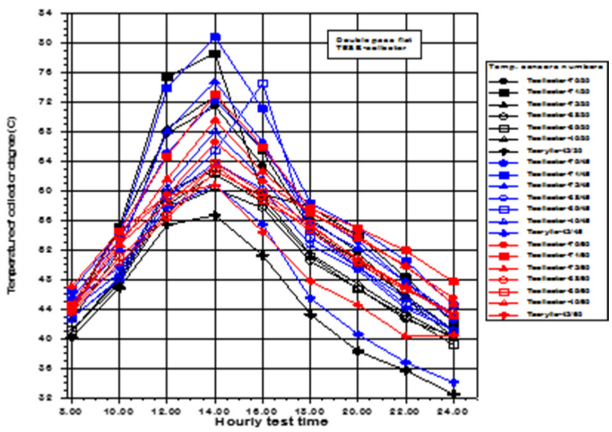

Fig. 18. Comparison between the SC absorber Temperature for double passes TESB collector and with different tilted angles.

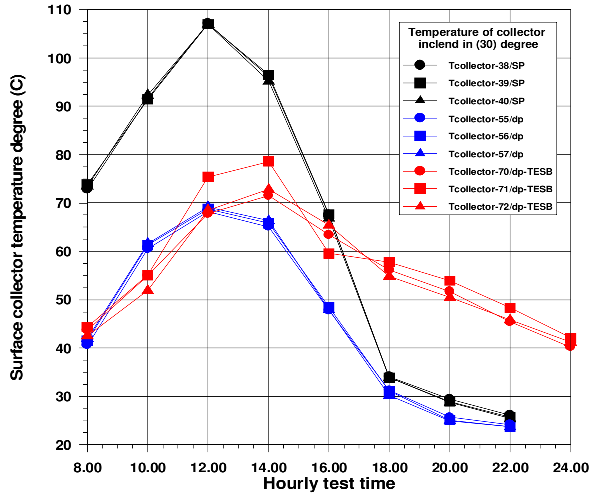

Fig. 19. Comparison between the SC temperatures for three different types at 30º tilted angle.

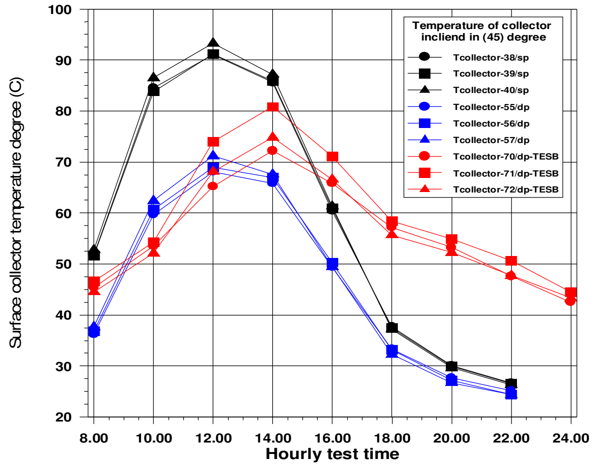

Fig. 20. Comparison between the SC temperatures for three different types at 45º tilted angle.

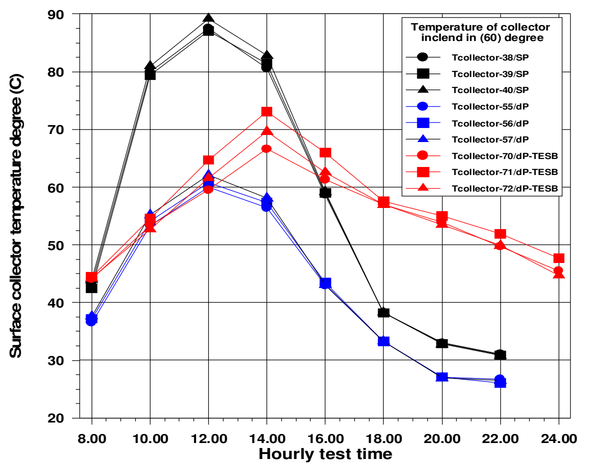

Fig. 21. Comparison between the SC temperature for three different types at 60º tilted angle

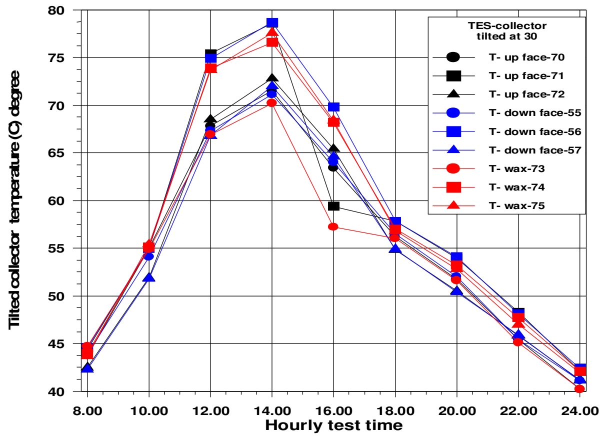

Fig. 22. Comparison between wax and surface temperature of TESB collector at 30° tilted angle

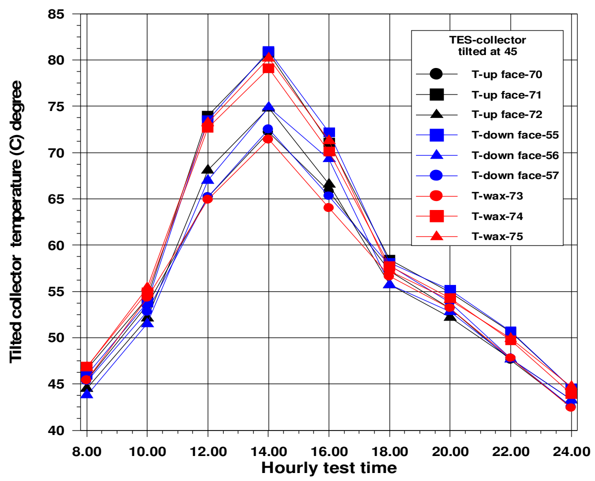

Fig. 23. Comparison between wax and surface temperature of TESB collector at 45° tilted angle.

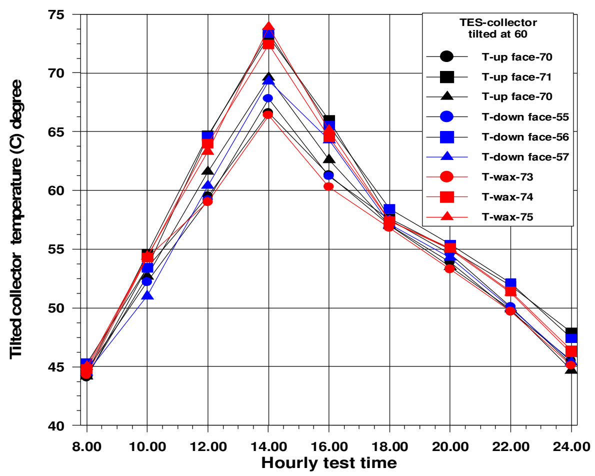

Fig. 24. Comparison between wax and surface temperature of TESB collector at 60° tilted angle.

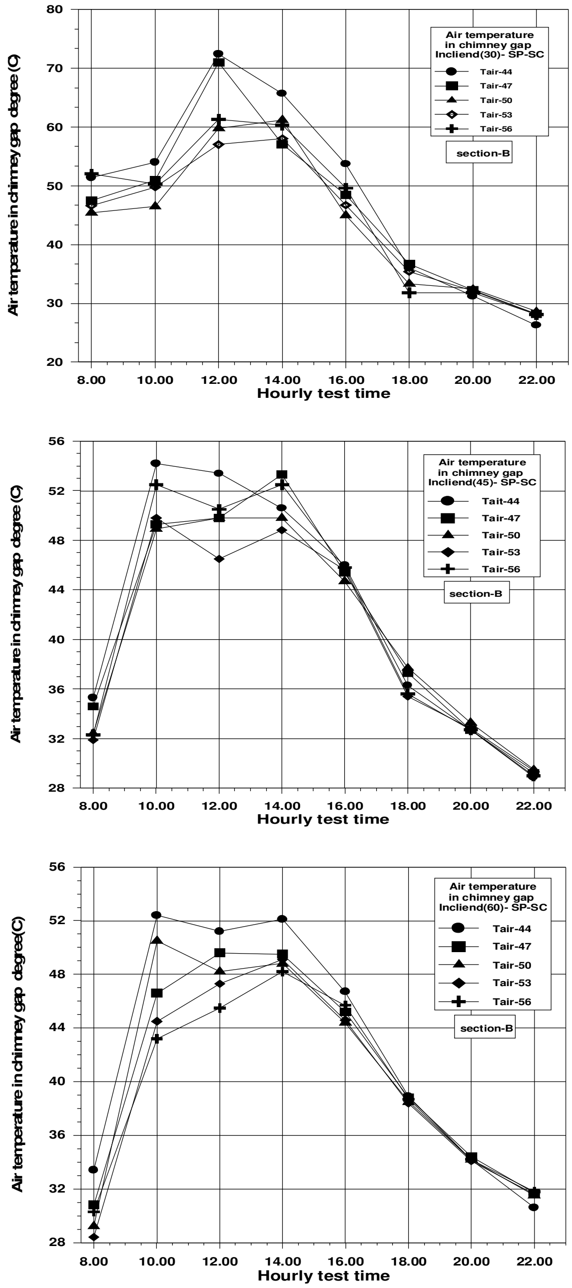

Fig. 25. Air temperature in single pass flat plate collector of SC in different sections and different angles.

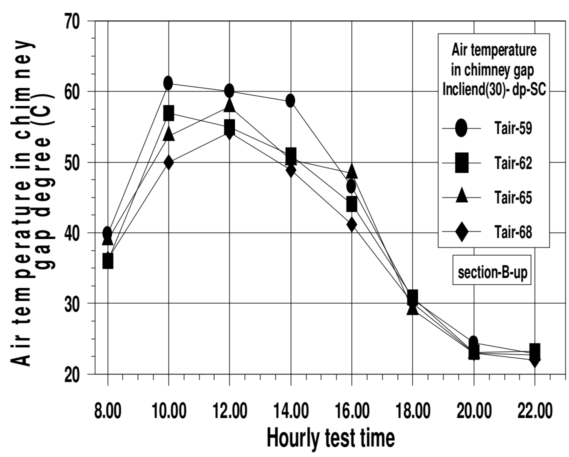

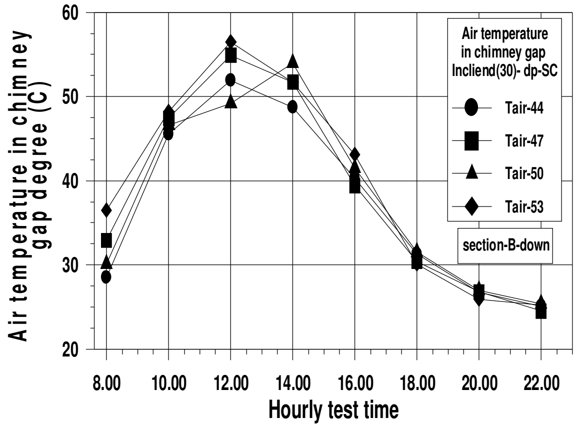

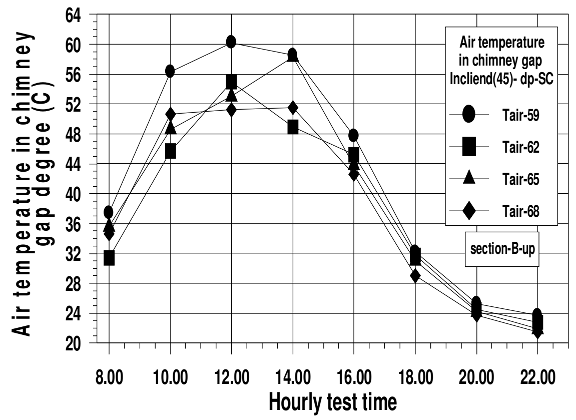

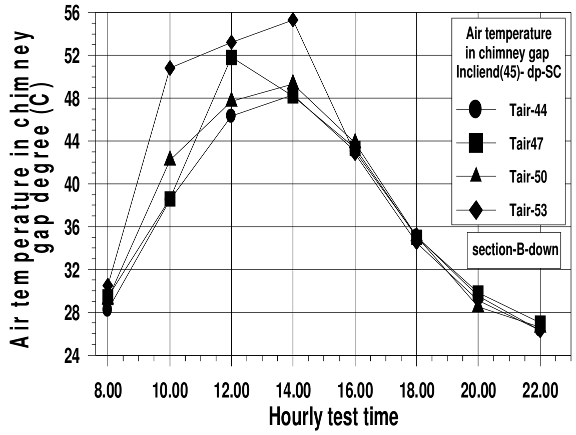

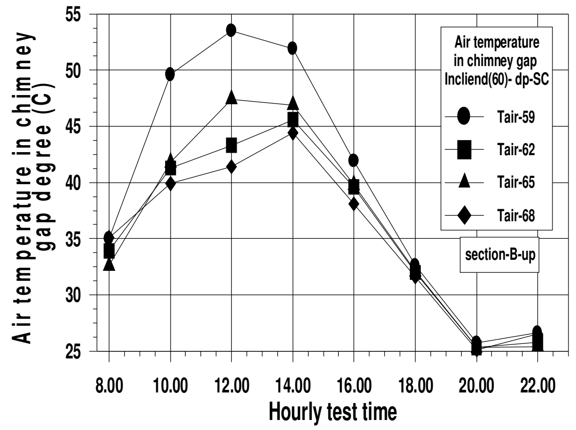

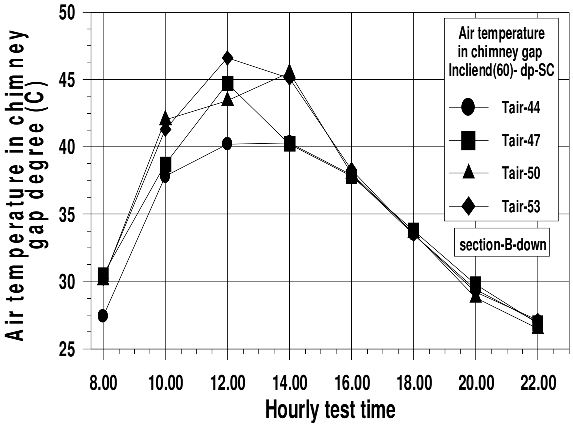

Fig. 26. Air temperature in double passes flat plate collector of SC in different sections and different angles.

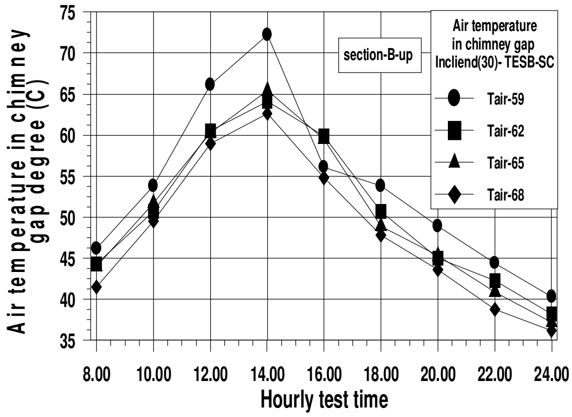

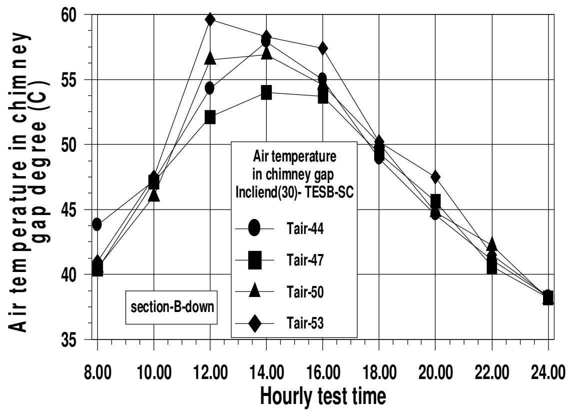

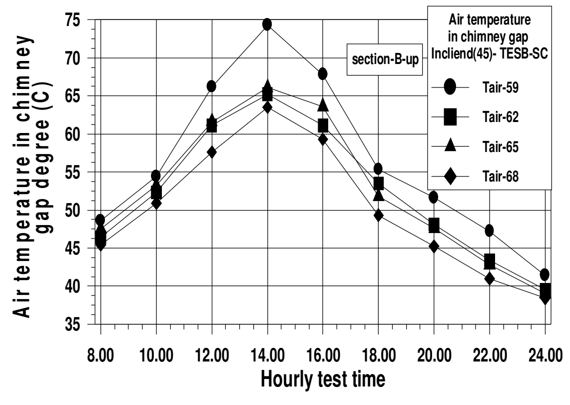

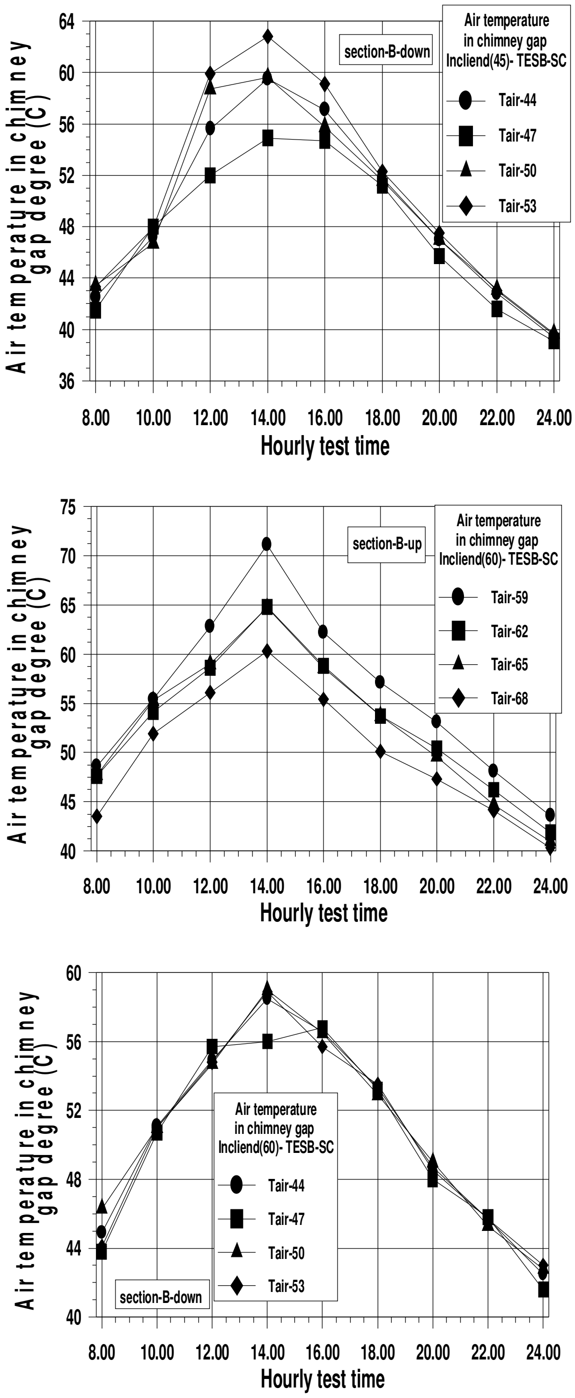

Fig. 27. Air temperature in double passes TESB collector of SC in different sections and different angles.

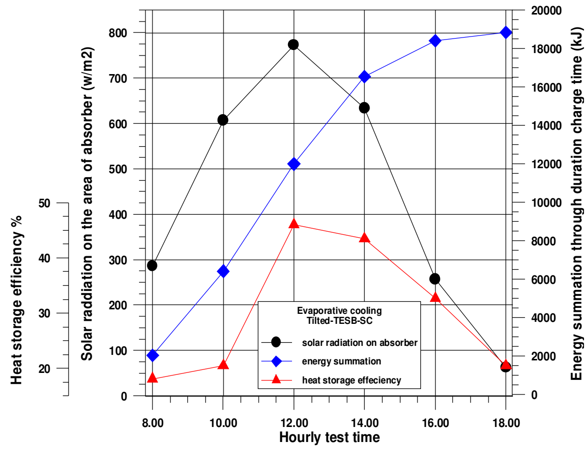

Fig. 28. Solar radiation, energy summation and heat storage efficiency.

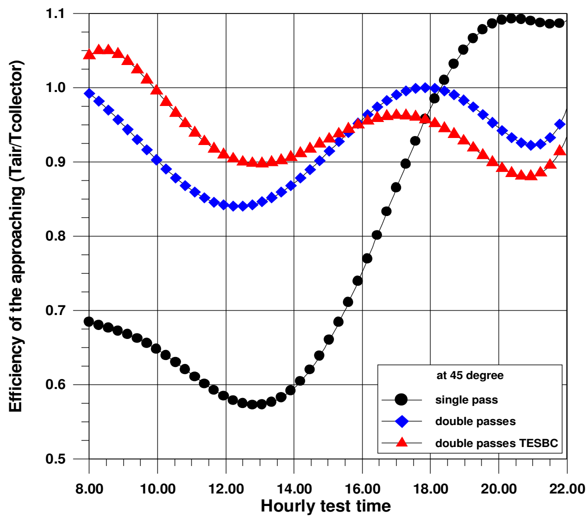

Fig. 29. Ratio of temperature for air in gap to the collector surface temperature for different collector types.

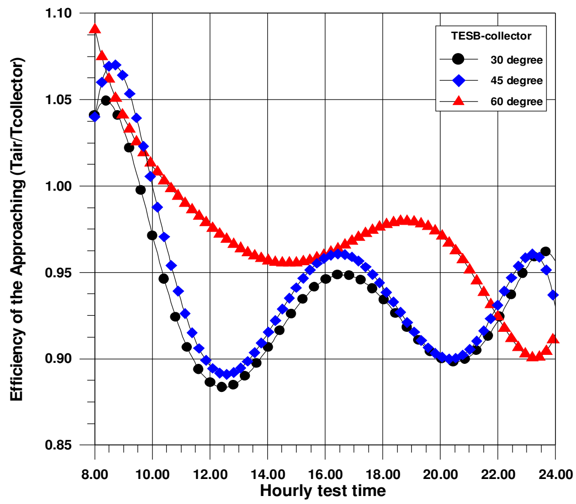

Fig. 30. Ratio of temperature for air in gapto the TESB collector surface temperature for different working angles.

08:00 AM 10:00 AM 12:00 PM 02:00 PM 04:00 PM 0:600 PM 08:00 PM 10:00 PM 12:00 AM

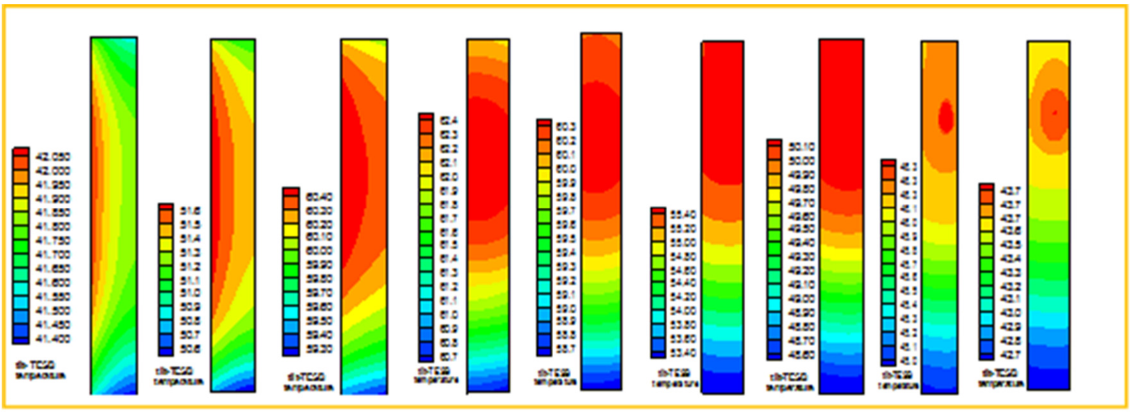

Fig. 31. Temperature distribution inside thermal energy storage box at charge and release heat energy.

Nomenclatur

A	Area
a_E, a_W, a_N,	Coefficient in the discretization
ar	Dimensionless aspect ratio
C_d	Discharge coefficient
C_p	Specific heat
CFD	Computational fluid dynamic
CFM	Copper foam matrix
CV	Control volume
FVM	Finite volume method
g	Gravitational acceleration
h	Enthalpy , height
h	Heat transfer coefficient
h_{fu}, h_{fs}	Latent heat of fusion
hr	Hour
I_{beam}	beam solar radiation
k	Thermal conductivity
k_{eff} ,$k_{PCM-CFM}$	Effective thermal conductivity of the PCM-embedded copper foam matrix
L	Length
m, $\dot{m}$	Mass, mass flow rate
P	Point
PCM	Phase change material
ppi	Porous per inch
PW	Paraffin wax
q''	Heat flux
Q'''	Internal heat generation rates
S	Source term
S	Heat generation
T, t	Temperature, time
TESM	Thermal energy storage material
$\dot{V}$	Volume flow rate

Greek letters

ρ	Density
τ	Width of melting zone
α	Diffusivity
θ	Solar chimney tilt angle
η	Heat Storage Efficiency
Δ_x, Δ_y	Dimensions of the computational cell
$\delta_e, \delta_w, \delta_n,$	Inter-nodal distance

Subscripts

av	Average
e	Control-volume face between *P*
E	Neighbor in the positive *x* direction
eq	Equivalent
P, N, S,	Refers to grid nodes
n, s, e, w	Refers to cell face
i,j	Location of point in Cartesian grid
l, 2	Liquid
m	Mushy, melting
n	Number of sections in material
N	Neighbor in the positive *y* direction
P	Central grid point under
s	Control-volume face between *P*
S	Neighbor in the positive *y* direction
s, 1	Solid
sl	Liquid –solid
w	Control-volume face between *P*
W	Neighbor in the positive *x* direction

9. References

[1] H. Kotani, S. D. Sharma, Y. Kaneko, T. Yamanaka, and K. Sagara," Development of Solar Chimney with Built-In Latent Heat Storage Material for Natural Ventilation", Department of Architectural Engineering, Graduate School of Engineering, Osaka University 2-1, Yamadaoka, (2005), pp. 565-0871, Suita Osaka, Japan.

[2] Mustafa B. Al-Hadithi "Use of Phase Change Material in Residential Walls to Reduce Cooling Load", AJES, Vol.4, No.1, (2011), pp.72-86.

[3] Alkilani Mahmud, Sopian K., Alghoul M. A., and Mat Sohif, "Using a Paraffin Wax-Aluminum Compound as a Thermal Storage Material in a Solar Air Heater", ARPN Journal of Engineering and Applied Sciences, Vol. 4, No. 10, December, (2009), pp.74-77.

[4] M. E. Poulad, and Alan Fung, "Potential benefits from Thermosyphon- PCM (TP) integrated design for buildings applications in Toronto", Proceedings of eSim 2012: The Canadian Conference on Building Simulation.

[5] Karima E. Amori and SaifWatheq Mohammed, "Experimental and numerical studies of solar chimney for natural ventilation in Iraq", Energy and Buildings 47, (2012), pp.450-457.

[6] Pathik H. Vadwala, "Thermal Energy Storage in Copper Foams filled with Paraffin Wax", M.ScThesis, Mechanical & Industrial Engineering, University of Toronto, 2011.

[7] K. Boomsma and D. Poulikakos, "On the effective thermal conductivity of a three-dimensionally structured fluid-saturated metal foam", International Journal of Heat and Mass Transfer 44 (2001), pp. 827-836.

[8] Yuan Tian, "Heat Transfer Enhancement in Phase Change Materials (PCMs) by MetalFoams and Cascaded Thermal Energy Storage", PhD, Thesis, University of Warwick. 2012.

[9] Y. Tian and C.Y. Zhao, "Thermal and Exergetic Analysis of Metal Foam-enhanced Cascaded Thermal Energy Storage (MF-CTES)", International Journal of Heat and Mass Transfer 58, (2013), pp. 86–96.

[10] Anil W. Date," Introduction to Computational Fluid Dynamics", Indian Institute of Technology, Bombay, Cambridge University, Press 2005.

[11] Kau-Fui Vincent Wong, "Intermediate Heat Transfer", University of Miami Coral Gables, Florida, U.S.A., Marcel Dekker, Inc., 2003.

[12] "3-D Heat transfer problem", Texas advanced computer center, the University of Texas at Austin.

[13] Mahesh Prakash,Özden F. Turan, and Graham R. Thorpe. "Program NATCON: For the numerical of Buoyancy-driven laminar and turbulent flows in differentially heated cavities", a new school of thought, Victoria University, Melbourne Australia, 2006.

[14] Sajda, F. S., "Simulation of trombe wall in mixed convection plus conduction", MS.C, thesis, University of Technology, Technical Education Dep., 2005.

[15] Ahmed K. Taha, "Simulation of Heat Storage and Heat Regeneration in Phase Change Material", MSc thesis, University of Baghdad, 2010.

تحليل السلوك غير المستقر لطاقة الأشعة الشمسية المخزنة في المادة ثنائية الطور المدعمة برغوة النحاس باستخدام طريقة السعة الحرارية المكافئة كنموذج خزن

طالب كشاش مرتضى* حسين مجيد صالح علي داود سلمان*****

*قسم الهندسة الميكانيكية/ كلية الهندسة/ جامعة مؤته / الاردن
**قسم الهندسة الكهروميكانيكية/ الجامعة التكنولوجية/ العراق
*** قسم الهندسة الميكانيكية/ الجامعة التكنولوجية/ العراق
*البريد الالكتروني: talib_km@yahoo.com
**البريد الالكتروني: hussein_maj@yahoo.com
**البريد الالكتروني: aligaphory@yahoo.com

الخلاصة

تم استخدام الشمع البرافيني المدعم برغوة النحاس بوصفه مادة خزن حراري وتوظيفه ضمن المدخنة الشمسية ثنائية المجرى للحصول على تأثير التهوية او التهوية مع التبريد ألترطيبي خلال وبعد غياب الشمس. المدخنة الشمسية تم تنصيبها ضمن الجدار المواجه الى الجنوب لغرفة الاختبار المعزولة حراريا والتي تم فيها اختبار المدخنة الشمسية ضمن زاوية عمل مختلفة (60°, 45° and 30°) ولثلاثة انواع من المداخن الشمسية وهي المدخنة ذات الممر الهوائي الأحادي والمزدوج فضلا عن المدخنة ذات الممر الهوائي المزدوج ذي ماص حراري بشكل صندوق خزن حراري يحوي مادة الشمع البرافيني المدعم برغوة النحاس. تم بناء برنامج محاكاة لحل النموذج الحسابي للجزء غير المستقر (العابر) وذلك باستخدام طريقة الحجوم المحددة، حيث ان انتقال الحرارة وخزنها تم تمثيله عن طريق المعادلات الحاكمة (معادلة) الطاقة والتي تم استخدامها بشكل دالة لدرجة الحرارة، كذلك تم توظيف طريقة الحرارة النوعية المكافئة لوصف خزن الحرارة في المنطقة الثنائية الطور الانتقالية والتي تعد من أسهل الطرائق وادقها المستخدمة في وصف انتقال الحرارة وخزنها في المادة ثنائية الطور والمتحوله من الصلب الى السائل وبالعكس وبفعل كسب او فقدان الحرارة. النتائج العملية أشارت الى زيادة الموصلية الحرارية بعشرة اضعاف للمادة ثنائية الطور بعد تدعيمها برغوة النحاس، بينما تأثير التهوية يبقى فعالا ولمدة ساعات مع تأثير اقل بعد غياب المصدر الحراري (الشمس) وبالاعتماد على السعة الحرارية المخزونة. بينت النتائج العملية ان اكبر معدل تدفق كتلي للهواء تم تسجيله بمقدار 36.651 kJ/hr. والتي عندها قيمة معامل التدفق المحسوب لهذه المنظومة بمقدار 0.371. كذلك اظهرت النتائج العملية أفضل زاوية عمل 60°-45°، وان نسبة اقتراب درجة حرارة الهواء من درجة حرارة السطح الماص والتي اظهرت اعلى قيمة عند المدخنة الشمسية ثنائية المجرى, اظهرت النتائج العملية ان المدخنة الشمسية ذات مواد الخزن الحرارية تظهر تأثير لفترة طويلة حتى بعد غياب الشمس لكن مع تأثير حراري اقل نتيجة الحفاظ على درجة حرارة مستقرة تمثل درجة الانصهار للمادة الثنائية والتي تحدد فيها درجة الحرارة بالثبات على الرغم من اكتساب الحرارة، النتائج أشارت الى اعلى كفاءة لخزن الحرارة ضمن مادة الخزن المركبة وبمقدار 47% عند اعلى مقدار للإشعاع الشمسي $780W/m^2$ ضمن ظروف الاختبار عند وقت الاختبار 12:00 pm والسبب في ذلك يعود الى اكتساب الهواء المار في المدخنة جزء من الحرارة المخزنة لدوام استمرارية عمل المنظومة وهذا يحدث بسبب فرق درجات الحرارة , بينما سجل مجموع الطاقة خلال مدة الشحن الحراري بمقدار 18460 kJ . النتائج الحسابية أظهرت سلوكا منطقيا لذوبان الشمع وتصلده خلال مدة شحن الحرارة واطلاقها بوجود الرغوة المعدنية، مع تقارب منطقي للنتائج النظرية من العملية وبمعدل خطا يصل الى 16.8% حيث تم اعتماد طريقة الحرارة النوعية المكافئة لحساب الحرارة المخزونة في المادة ثنائية الطور المدعمة برغوة النحاس.